Contribution from the Department of Chemistry,
Wayne State University, Detroit, Michigan 48202

Pulsed Photoacoustic Microcalorimetry in Aqueous Solutions. Intersystem Crossing Efficiencies and Bond Dissociation Energies of Chromium(III) Ammines[1]

Xiaoqing Song and John F. Endicott*

Received July 24, 1990

The pulsed photoacoustic microcalorimetric method has been used to characterize the excited-state processes that are induced by ligand field excitations of some chromium(III) complexes in aqueous solutions. As reference compounds, we have used several cobalt(III) and chromium(III) complexes that are photoinert for 460-nm irradiation and that have subnanosecond excited-state lifetimes. Experimental and theoretical transducer wave forms were critically compared by using Fourier transform methods. The observed transducer (Panametrics A110S) response was found to be insensitive to the decay characteristics of intermediate excited states, provided the intermediate excited-state lifetimes exceeded 300 ns. The technique was used to determine that intersystem crossing efficiencies (η_{isc} for $^4T_2 \rightarrow {}^2E$) were 1.03 ± 0.07 for some photoinert chromium(III) complexes that contain macrocyclic ligands and that have relatively long (^2E) excited-state lifetimes. For the photoactive $Cr(NH_3)_6^{3+}$ and $Cr(NH_3)_5Cl^{2+}$ complexes, the amplitudes of the photoacoustic signals implied that the differences in Cr–NH_3 and Cr–OH_2 bond dissociation energies were 33 ± 10 and 24 ± 10 kJ mol^{-1}, respectively, in reasonable agreement with simple angular overlap arguments.

Introduction

In studies of reactive chemical systems one is often confronted with problems whose most convenient resolution would involve the measurement of a heat quantity. In many instances, as in the characterization of electronic excited states, the heat quantity in question is related to the initial stages of a sequence of elementary reaction steps, and it must be determined quickly. Several recent studies have shown that the photoacoustic detection methods employing high-frequency piezoelectric transducers and pulsed light sources can be used for fast, quantitative, and convenient heat measurements.[2-7]

Nonradiative molecular relaxation processes, whether vibronic excited-state relaxations or chemical rearrangements, are heat-producing processes that can be used in the quantitative characterization of a reactive system. For example, the efficiency with which a reactive, but metastable excited state is formed by means of a nonradiative cascade through higher energy excited states is an important factor in the determination of the overall efficiency of a photochemical process (see Figure 1), and it is a factor that must be determined in order that excited-state reaction patterns may be understood. When such metastable excited states differ from the ground state and from the initial excited state in spin multiplicity, the efficiency of forming such states is the intersystem crossing efficiency, η_{isc}.[8] Traditional approaches have inferred values of η_{isc} from bimolecular energy transfer and/or chemical scavenging techniques. Such approaches tend to be tedious and often subject to appreciable uncertainty. As a consequence there are only a few literature values of η_{isc}, and there have been very few determinations of η_{isc} for coordination complexes.

Much of the previous literature on photoacoustic microcalorimetry has used ultraviolet excitations of compounds in non-aqueous solutions (the very recent work of Goodman is an exception[6b]). This is partly a consequence of traditions for the study of UV-absorbing molecular substrates but is more observed because the quantitative photoacoustic measurements must be referenced to compounds of known photophysics and most of these reference compounds are water-insoluble aromatic or dye molecules. However, restrictions to UV excitations and non-aqueous solvents would prevent the technique from being generally useful, so we have been examining the extension of photoacoustic microcalorimetric techniques to studies employing visible excitations of substrates in aqueous solutions.

Despite the extensive studies of Cr(III) photophysics, fewer than a dozen intersystem crossing yields have been reported,[7a,9-11] and several of those are the result of earlier photoacoustic studies from this laboratory that employed UV excitations of Cr(III)–polypyridyl complexes in ethanolic solutions.[7a] We have now extended this work to visible excitations of the ligand field absorption bands of several Cr(III)–am(m)ine complexes in aqueous solutions. In the course of this work, we have examined both photoinert and photoactive Cr(III) complexes, and we have determined the heat changes that accompany photoaquation in ammine complexes.

Experimental Section

Materials. The synthesis and characterizations of chromium(III) complexes used in this study are reported elsewhere.[12] Literature methods were used for the synthesis and characterization of [Co(sep)]Cl_3,[13,14] [Co([9]aneN$_3$)$_2$]Cl_3,[15] and [Co(sen)]Cl_3.[16] The complex salts were metathesized to perchlorate or trifluoromethanesulfonate salts, purified, and characterized by elemental analysis, IR, UV-vis, and/or NMR spectroscopy.

(1) Partial support of this research by the Division of Chemical Sciences, Office of Basic Energy Sciences, Office of Energy Research, U.S. Department of Energy, is gratefully acknowledged.

(2) (a) Patel, C. K. N.; Tam, A. C. *Rev. Mod. Phys.* **1981**, *53*, 517. (b) Tam, A. C. *Rev. Mod. Phys.* **1986**, *58*, 381.
(3) (a) Rothberg, L. J.; Simon, J. D.; Bernstein, M.; Peters, K. S. *J. Am. Chem. Soc.* **1983**, *105*, 3464. (b) Bernstein, M.; Simon, J. D.; Peters, K. S. *Chem. Phys. Lett.* **1983**, *100*, 241. (c) Rudzki, J. E.; Goodman, J. L.; Peters, K. S. *J. Am. Chem. Soc.* **1985**, *107*, 7849.
(4) (a) Hawari, J. A.; Griller, D.; Chatgiliabglu, C. *J. Am. Chem. Soc.* **1987**, *109*, 5267. (b) Burkey, T. J.; Majewski, M.; Griller, D. *J. Am. Chem. Soc.* **1986**, *108*, 2218.
(5) (a) Blimes, G. M.; Tocho, J. O.; Braslavsky, S. E. *J. Phys. Chem.* **1989**, *93*, 6696; (b) *J. Phys. Chem.* **1988**, *92*, 5958. (c) Aramendia, P. F.; Kreig, M.; Nitsch, C.; Bittersmann, E.; Braslavsky, S. E. *Photochem. Photobiol.* **1988**, *48*, 187.
(6) (a) Herman, M. S.; Goodman, J. L. *J. Am. Chem. Soc.* **1989**, *111*, 1849. (b) Goodman, J. L.; Herman, M. S. *Chem. Phys. Lett.* **1989**, *163*, 417.
(7) (a) Lynch, D.; Endicott, J. F. *Inorg. Chem.* **1988**, *27*, 2181. (b) Lynch, D.; Endicott, J. F. *Appl. Spectrosc.* **1989**, *43*, 826.
(8) Birks, J. B. *Photophysics of Aromatic Molecules*; Wiley: New York, 1970.
(9) Kirk, A. D. *Coord. Chem. Rev.* **1981**, *39*, 225.
(10) Endicott, J. F.; Ramasami, T.; Tamilarasan, R.; Lessard, R. B.; Ryu, C. K.; Brubaker, G. R. *Coord. Chem. Rev.* **1987**, *77*, 1.
(11) Foster, L. S. *Chem. Rev.*, **1990**, *90*, 331.
(12) (a) Ryu, C. K.; Lessard, R. B.; Lynch, D.; Endicott, J. F. *J. Phys. Chem.* **1989**, *93*, 1752. (b) Lessard, R. B.; Endicott, J. F.; Perkovic, M. W.; Ochromowycz, L. M. *Inorg. Chem.* **1989**, *28*, 2574. (c) Lessard, R. B.; Heeg, M. J.; Buranda, T.; Perkovic, M. W.; Schwarz, C. L.; Endicott, J. F. *Inorg. Chem.* To be submitted for publication. (d) Perkovic, M. W.; Endicott, J. F. *J. Phys. Chem.* **1990**, *94*, 1217. (e) Perkovic, M. W. Ph.D. Dissertation, Wayne State University, 1990.
(13) Creaser, I. I.; Harrowfield, J. MacB.; Herit, A. J.; Sargeson, A. M.; Springborg, J.; Geue, R. J.; Snow, M. R. *J. Am. Chem. Soc.* **1977**, *99*, 3181.
(14) Ligand abbreviations: [9]aneN$_3$ = 1,4,7-triazacyclononane; [([9]aneN$_3$)CH$_2$–]$_2$ = 1,2-bis(1,4,7-triaza-1-cyclononyl)ethane; [14]aneN$_4$ = 1,4,8,11-tetraazacyclotetradecane; [15]aneN$_4$ = 1,4,8,12-tetraazacyclopentadecane; sen = 4,4′,4″-ethylidynetris(3-azabutan-1-amine; sep = (*S*)-1,3,6,8,10,13,16,19 octaazabicyclo[6.6.6]eicosane; TAP[9]aneN$_3$ = 1,4,7-tris(aminopropyl)-1,4,7-triazacyclononane.
(15) Wieghardt, K.; Schmidt, W.; Herrmann, W.; Kuppers, H.-J. *Inorg. Chem.* **1983**, *22*, 2953.
(16) Geue, R. J.; Searle, G. H. *Aust. J. Chem.* **1983**, *36*, 927.

0020-1669/91/1330-2214$02.50/0

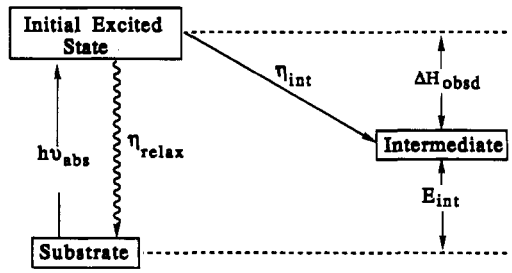

Figure 1. Schematic diagram illustrating the use of fast heat measurements (ΔH_{obsd}) in characterizing an intermediate: (a) if E_{int} is independently known, the efficiency of intermediate formation can be determined (e.g., η_{int}), or (b) if η_{int} is known, E_{int} may be determined.

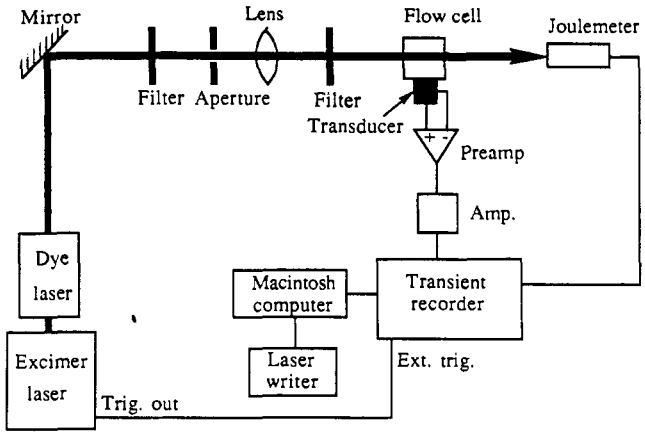

Figure 2. Schematic diagram of the pulsed photoacoustic system used in this study.

Caution! The perchlorate salts used in this study are potentially explosive and must be handled with care.

Techniques. a. Instrumentation. Our version of the pulsed photoacoustic calorimetric technique has been described elsewhere.[7] In the present study we have used a Lambda Physik EMG 102 excimer laser pumped Lambda Physik FL 3001 E/3002 EC dye laser to obtain 462.2-nm excitation pulses of about 8 ns pulse width and laser pulse energy of less than 100 μJ. A schematic diagram of this system is shown in Figure 2. A flow cell was used for photoactive samples, and the flow rate was found to have no significant effect on the photoacoustic waveform. A 5-MHz transducer, Panametrics Model A110S, was used as the detector, coupled externally to the sample cuvette by a thin layer of grease. Signals were collected and averaged (64 shots per experiment) on a Gould-Biomation 4500 transient recorder. The initial peak amplitude, the voltage difference between the first positive peak maximum and the trough of the following peak, was used as a measure of the amplitude of the pressure wave generated by nonradiative relaxation of the photoexcited sample. In some instances, we have calculated the Fourier transform of the photoacoustic signal (see below) and used the amplitude of the peak in the frequency domain as a measure of the heat signal. The dye laser output was calibrated with respect to the atomic emissions of Fe between 384 and 516 nm by using a Perkin-Elmer ATOMAX LAMP and a Hilger-Engis 0.6-m monochromator.

Our luminescence detection system has been described elsewhere.[12] Samples were excited with monochromatic radiation from a Molectron UV-1010 pumped DL-14 tunable dye laser. Lifetime determinations were made for samples at 25 °C by using a Hammamatsu R955-PMT coupled to a Gould-Biomation 4500 digital oscilloscope for digitization and signal averaging and interfaced to a Dell System 200 computer for data manipulation and curve fitting with software developed by On Line Instrument Systems, Inc. (Jefferson, GA).

b. Waveform Modeling and Fourier Transforms. The equation proposed by Peters and co-workers[3]

$$V_t = \frac{h_0 A \omega_a/\tau}{4\pi r_0[\omega_a^2 + (1/\tau')^2]}\left\{e^{t/\tau} - e^{-t/\tau_0}\left[\cos(\omega_a t) - \frac{1}{\omega_a \tau'}\sin(\omega_a t)\right]\right\} \quad (1)$$

has been used to numerically model the expected transducer response. In eq 1, V_t is the measured photoacoustic signal amplitude at time t that results from a single heat source of characteristic lifetime τ and generates an amount of heat $h_0 = \eta_{nr}E_p(1 - 10^{-A})$, where η_{nr} is the nonradiative relaxation efficiency, E_p is the laser pulse energy, $\omega_a = 2\pi\nu_a$ (this differs slightly from the usage in ref 3) where ν_a is the resonant frequency of the transducer, τ_0 is the relaxation time of the transducer, r_0 is the distance between the laser beam and the transducer, and $1/\tau' = 1/\tau - 1/\tau_0$. For transients whose lifetimes are much shorter than the time-resolved detection limits of the transducer (i.e., $\tau \leq 1$ ns), eq 1 reduces to

$$V_{pa} = K\eta_{pnr}E_{abs} = K\eta_{pnr}E_p(1 - 10^{-A}) \quad (2)$$

where V_{pa} is the photoacoustic (PA) signal amplitude and η_{pnr} is the heat efficiency of prompt ($\tau < 1$ ns) nonradiative relaxation processes. The value of η_{pnr} is determined as the ratio of the heat produced to the laser pulse energy, and K is an experimental constant that needs to be calibrated by using standard, or reference, compounds.

We have also modeled the photoacoustic transducer response in a system with two heat sources, one a "prompt" (Δ function) heat source (i.e., with lifetime $\tau_1 \ll 1$ ns) and the other a "slow" heat source (with lifetime τ_2), which spans a range of frequencies around the inherent detector frequency. This modeling indicated that the wave amplitude should be directly proportional to the amplitude of the prompt heat pulse when $\tau_2 \gg \nu_a^{-1}$, while the wave amplitude became proportional to the sum of the amplitudes for the prompt and slow heat pulses when $\tau_2 \ll \nu_a^{-1}$. In the intermediate time regime, where $\tau_2 \sim \nu^{-1}$, there should be a detectable phase shift, and the photoacoustic signal amplitude assumed intermediate values (see Table I). These variations in photoacoustic signal amplitudes differed in phase from a single prompt heat pulse, with the phase shift maximizing when $\tau_2 = \nu_a^{-1}$. The amplitude of the maximum calculated phase shift depended on the ratio of heat amplitudes (h_0) of the prompt and slow heat pulses.

It is sometimes helpful to be able to compare time domain and frequency domain signals, since the frequency domain signal should be free of any problems arising from phase shifts. We have used the fast Fourier transform technique to obtain the frequency domain spectrum from experimental or modeled time domain wave forms. The approach is very similar to that used in Fourier transform NMR, in which the transformed NMR spectrum will give all the frequency components that contribute to the FID signal. Similarly, the Fourier transform of the time-domain photoacoustic wave form should also give us all the frequency components that compose the photoacoustic wave form.

The time-domain representation, $h(t)$, and the frequency-domain representation, $H(f)$, of a function can be related to one another through the transformations[17]

$$h(t) = \int_{-\infty}^{\infty} H(f)\, e^{-2\pi i f t}\, df$$

$$H(f) = \int_{-\infty}^{\infty} h(t)\, e^{2\pi i f t}\, dt$$

In our experiments the function $h(t)$ was sampled at evenly spaced intervals in time, Δ. As a consequence, the sequence of sampled values becomes

$$h_n = h(n\Delta), \quad \text{for } n = \ldots, -3, -2, -1, 0, 1, 2, 3, \ldots$$

For a finite set of N consecutively sampled values, $h_k = h(t_k)$, where t_k

Table I. Comparison of the Calculated Relative Peak Amplitudes of the Photoacoustic Signal (V_{pa}) and Its Fourier Transform (I) for (A) Different Heat Production Efficiencies (η_{pnr}) of a Prompt Heat Source (τ = 10 ps) and B, Signal Behavior in a System Containing both a Prompt Heat Source and a Metastable, Heat-Producing Intermediate State

part A[a]			part B[b]			
η_{pnr}	V_{pa}	I (I/I_s)[c]	τ_2, ns	V_{pa}/V_s[c]	I/I_s[c]	% dev[d]
0.100	0.095 393	0.898 (0.100)	10	0.976	0.984	−0.8
0.200	0.190 791	1.80 (0.200)	50	0.769	0.723	6.0
0.300	0.286 186	2.69 (0.300)	100	0.614	0.516	16.0
0.400	0.381 581	3.60 (0.401)	200	0.488	0.396	24.9
0.500	0.467 976	4.49 (0.500)	400	0.416	0.354	14.9
0.600	0.572 372	5.39 (0.600)	500	0.400	0.350	12.5
0.700	0.667 767	6.29 (0.700)	1000	0.369	0.342	7.3
0.800	0.763 162	7.19 (0.801)	2000	0.355	0.340	4.2
0.900	0.858 558	8.08 (0.900)	3000	0.350	0.340	2.9
1.000	0.953 953	8.98 (1.00)	5000	0.345	0.340	1.4

[a] Single, prompt heat pulse with τ = 10 ps. [b] Two heat sources, one propmt with τ_1 = 10 ps, the other with variable τ_2. For the prompt heat source $\eta_{pnr}(1)$ = 0.34; for the second heat source η_{nr} = 0.67. [c] V_s is the wave form amplitude for a short-lived transient with τ = 10 ps and η_{pnr} = 1.0; and I_s is the peak intensity of its Fourier transform spectrum. [d] % dev = $[(V_{pa}/V_s) - (I/I_s)]/(V_{pa}/V_s)$.

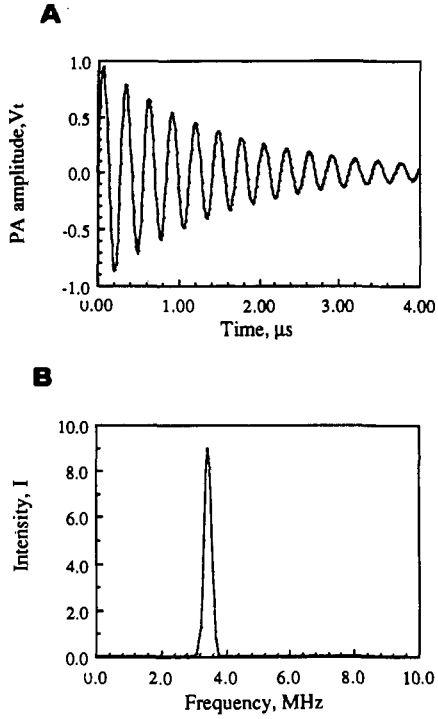

Figure 3. Theoretical transducer wave form (a) and its Fourier transform (b). The theoretical wave form was calculated by using eq 1 with ν_a = 3.52 MHz and τ_0 = 1.5 μs.

= $k\Delta$ and k = 0, 1, 2, ..., N − 1. For such a set, the sampling rate is defined as the reciprocal of the time interval, and the Fourier transform is estimated only at discrete frequency values.[17]

$$f_n = n/N\Delta, \quad n = -N/2, ..., N/2$$

For a single real function, subroutine REALFT (DATA, N, ISIGN)[18] was used as well as subroutine FOUR1 (DATA, NN, ISIGN). This routine will take a real data set h_j (j = 0, 1, ..., N − 1), split it into two data sets $h_j = (f(2j) + if(2j + 1)$ (j = 0, ..., [N/2] − 1) and return a complex array $H_n = F^e_n + iF^o_n$ (n = 0, ..., [N/2] − 1) with

$$F^e_n = \sum_{k=0}^{(N/2)-1} f_{2k} e^{2\pi ikn/(N/2)}$$

$$F^o_n = \sum_{k=0}^{(N/2)-1} f_{2k+1} e^{2\pi ikn/(N/2)}$$

where F^e_n and F^o_n represent the real (even numbered) and imaginary (odd numbered) parts of the data set, respectively, in the returned Fourier transform complex array. Alternatively, Fast Sine (subroutine SINFT (Y, N)) and cosine (COSFT (Y, N, ISIGN))[18] transform methods were also employed to get the imaginary part and the real part of the Fourier transform, respectively. The two methods gave the same result.

The complex spectrum, $C(v)$, can be represented by the sum of a purely real part, $R(v)$, and a purely imaginary prt, $I(v)$, so that $C(v) = R(v) + iI(v)$. The amplitude spectrum $S(v)$ can be obtained from the complex output $C(v)$ after phase correction. This can be done by calculating the square root of the power spectrum, $P(v) = [C(v)]C^*(v)$, so that

$$S(v) = [[C(v)]C^*(v)]^{1/2} = [R(v)^2 + I(v)^2]^{1/2}$$

In the actual calculation, the time-domain photoacoustic wave form (310 data points) was "padded"[17] with 202 zero amplitude numbers, producing a data set of N = 512 real data points. This data set was then apodized[16] by using the four-term Blackmann–Harris (BH) method[17,19] on both ends of the photoacoustic waveform based on

$$\mathrm{BH}(x) = A_0 + A_1 \cos(\pi N/L) + A_2 \cos(\pi 2N/L) + A_3 \cos(\pi 3N/L)$$

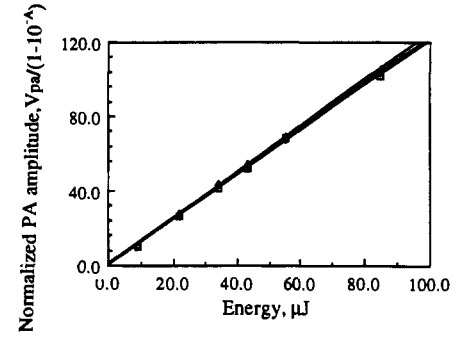

Figure 4. Typical calibration curve for the photoacoustic system in which the normalized PA signal, $V_{pa}/(1 - 10^{-A})$, is plotted against the pulse energy, E_p. Coordination complex samples were dissolved in water containing 5 × 10^{-3} M HCF_3SO_3 to obtain an absorbance of 0.023 at 462.2 nm. Complexes employed were $Co([14]aneN_3)_2^{3+}$ (open squares), $Co(sen)^{3+}$ (solid diamonds) and $Co(sep)^{3+}$ (open triangles).

where N = 0, 1, ..., L and BH(x) is the BH function with A_0 = 0.358 75, A_1 = 0.488 29, A_2 = 0.141 28, A_3 = 0.011 68 and L = 256. The data segment, here of length 256, was multiplied (bin by bin) by the BH(x) function, which produced the apodized data set with the same number of data points as the original. This data set was then padded with 512 zeros, producing a final data set with 1024 points before the Fourier transform was computed.

We have used eq 1 to model the "ideal" Fourier transform spectrum of our transducer with ν_a = 3.50 MHz and τ_0 = 1.5 μs. This "ideal" transducer response is illustrated in Figure 3b. For a short lived transient (Δ function), the relative peak amplitude (for changes of incident intensity) of the Fourier transform spectrum is exactly the same as that of the time-domain photoacoustic wave form. However, if there is a relatively long-lived transient in the time-resolved region as well as a very short-lived transient, the signal amplitude and the intensity of the corresponding Fourier transform spectrum were found to have the same relative amplitudes (±3% deviation) when $\tau < 0.1\nu_a^{-1}$ and when $\tau > 10\nu_a^{-1}$. The relative intensity of the transformed signal was smaller than the photoacoustic signal amplitude in the intermediate time regime, with the discrepancy reaching about 25% when $\tau \approx \nu^{-1}$ (see Table I).

c. Sample Solutions and Photoacoustic Measurements. All samples were at ambient temperatures, in aerated solutions. Sample solutions were prepared so that the absorbance at the excitation wavelength was approximately 0.1 in the 1 cm path length sample cell.

The photoacoustic signal amplitudes were determined for each sample by using a range of excitation intensities. The excitation pulse energy was varied by using neutral density filters (100, 70, 50, 40, 25, and 13% transmittance), and a calibration curve (see Figure 4) was generated for each compound. The slopes S_i (i = sample or reference) of the linear correlation lines (or of the resolved first-order component when the lines were curved; see comments in Results section) were used to determine the relative amount of heat, h_s, generated following excitation of each sample. The reference compounds employed in this study all returned the total energy of excitation promptly to the solution as heat, h_r. Since this can be equated to the laser pulse energy absorbed, E_p, the efficiency of heat production was η_{pnr} = 1.0 and eq 2 reduced to $V_{pa} = K(1 - 10^{-A})E_p$. Figure 4 illustrates the calibration procedure; a value of K = 24.2 ± 0.2 mv/μJ was inferred from these calibrations. Similar plots for samples investigated were used to obtain $S_{sample} = \eta_{pnr}K$, where S_{sample} is the slope of the plot of the normalized PA signal, $V_{pa}/(1 - 10^{-A})$, vs E_p.

The transducer response characteristics were experimentally determined by using a photoinert substrate, $Cr([9]aneN_3)_2^{3+}$,[20] whose metastable excited-state lifetime τ_2 could be varied from much longer to much shorter than ν_a^{-1} by altering the pH of the sample solution.

Results

A. Calibration of the Transducer Response. 1. Reference Compounds. We have used several cationic coordination complexes as reference compounds to calibrate the photoacoustic wave form amplitude. The compounds suitable for this purpose must have very short (less than 1 ns) intermediate excited-state lifetimes and they must be photoinert under the conditions employed. Cobalt(III) am(m)ine complexes are known to have very short excited-state lifetimes and very small product yields ($\ll 10^{-3}$) when

(17) Champency, D. C. *Fourier Transforms and their Physical Applications*; Academic Press: New York, 1973.
(18) Press, W. H.; Flannery, B. P.; Teukolsky, S. A.; Vetterling, W. J. *Numerical Recipes*; Cambridge University Press: Cambridge, England, 1986.
(19) Harris, F. J.; *Proc. IEEE* **1978**, *66*, 51.
(20) Ditze, A.; Wasgetian, F. *J. Phys. Chem.* **1985**, *89*, 426.

Table II. Excited-State Lifetime τ, Energy E, Prompt Nonradiative Efficiency η_{pnr}, and Intersystem Crossing Efficiency η_{isc} for Reference Compounds and Cr(III) Macrocyclic Complexes

complex	$\tau(^2E)$, μs	$E(^2E)$, $cm^{-1}/10^3$	η_{pnr}	η_{isc}
$Co([9]aneN_3)_2^{3+}$ [a]	$\ll 10^{-3}$		1.00	
$Co(sen)^{3+}$ [a]	$\ll 10^{-3}$		1.00	
$Co(sep)^{3+}$ [a]	$\ll 10^{-3}$		1.00	
$Cr([9]aneN_3CH_2^-)_2^{3+}$	$\ll 10^{-3}$ [b]		1.00	
$Cr([9]aneN_3)_2^{3+}$	30.2[c]	14.72[c]	0.36	0.94 ± 0.05
trans-$Cr([14]aneN_4)(CN)_2^+$	361[d]	14.06[d]	0.28	1.11 ± 0.10
trans-$Cr([15]aneN_4)(CN)_2^+$	190[d]	14.06[d]	0.30	1.08 ± 0.05
$Cr(TAP[9]aneN_3)_2^{3+}$	179[c]	14.90[c]	0.28	1.05 ± 0.05

[a] The excited-state lifetimes of these reference compounds are much shorter than 1 ns so the prompt nonradiative efficiencies are all unity. See refs 11 and 12e. [b] Unpublished results.[11d] [c] Reference 12d. [d] See ref 12c.

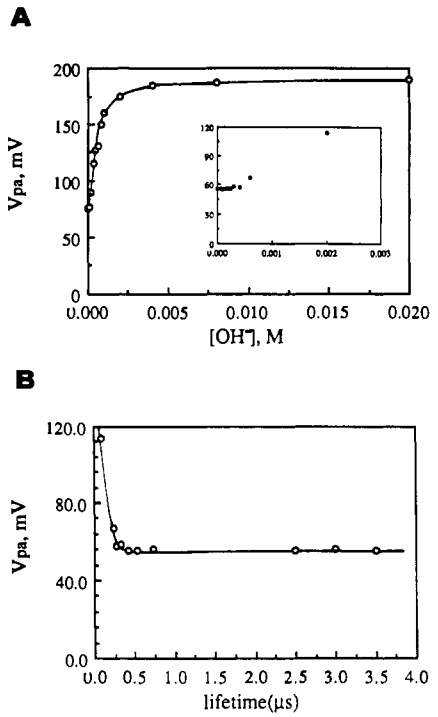

Figure 5. Experimental photoacoustic transducer response behavior as a transient excited state lifetime is varied: (a) signal amplitude as a function of hydroxide concentration in an aqueous sample solution of $Cr([9]aneN_3)_2^{3+}$; (b) signal amplitudes from the insert of part a plotted against the observed $(^2E)Cr([9]aneN_3)_2^{3+}$ excited state lifetimes.

these compounds are excited in their d–d absorption bands.[10,21] In addition to several Co(III) complexes, we have used $Cr[(9]-aneN_3)CH_2^-]_2^{3+}$, which has been shown to be nearly photoinert and to have a very short (≤25 ps) intermediate excited-state lifetime.[12d,e] The comparison of heat measurements in these systems is presented in Table II.

2. Experimental Examination of the Response of the Photoacoustic Signal to Variations in Intermediate Excited-State Lifetimes. We have varied the $(^2E)Cr([9]aneN_3)_2^{3+}$ lifetimes from 30 μs to about 0.1 μs by means of increases in [NaOH]. As the $[OH^-]$ in the sample solution was increased, the photoacoustic signal amplitude also increased to a maximum value, which was 2.5 times the signal amplitude in acidic solutions (Figure 5a). These variations in signal amplitude could be correlated with the independently measured $(^2E)Cr([9]aneN_3)_2^{3+}$ excited-state lifetimes, figure 5b, and establish that metastable intermediate state lifetimes of greater than 0.3 μs fall into the regime in which prompt and intermediate rates of heat production are clearly discriminated by our system. The ratio of the prompt signal amplitude in acidic solutions to the total amplitude in strongly basic solutions is 0.40, in reasonable agreement with $\eta_{pnr} = 0.36$ as listed in Table II. Thus these observations provide a nearly quantitative, independent confirmation of our procedures, in addition to the experimental determination of the transducer frequency response.

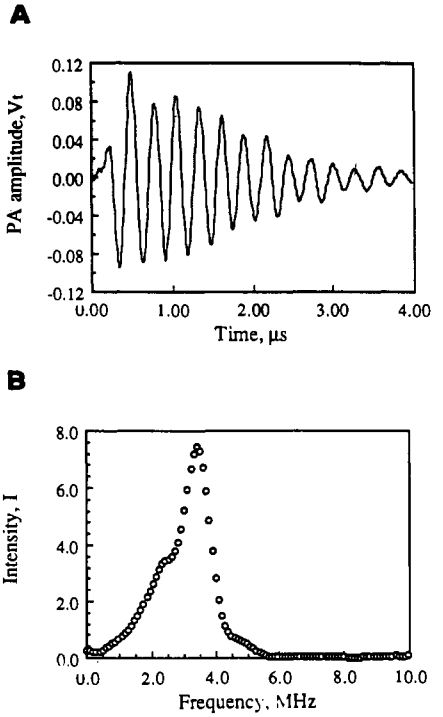

Figure 6. Comparison of the experimental photoacoustic signal wave form of $Co(sen)^{3+}$ (a) to its Fourier transform (b).

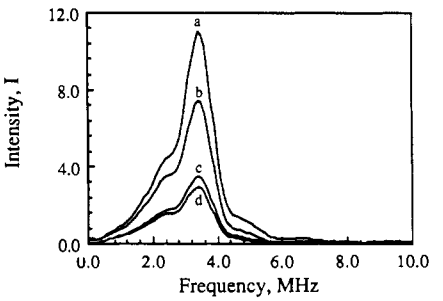

Figure 7. Comparison of the photoacoustic Fourier transform spectra of some coordination complexes with different $(^2E)Cr(III)$ excited-state lifetimes (τ_e): (a) $Cr(NH_3)_5NCS^{2+}$ (τ_2 = 270 ns); (b) $Co(sen)^{3+}$ (τ_2 < 1 ns); (c) $Cr(NH_3)_5CN^{2+}$ (τ_2 = 14 μs); (d) $Cr(NH_3)_6^{3+}$ (τ_2 = 2 μs). Sample solutions had different absorbances at 460 nm.

3. Fourier Transform Analysis of the Experimental Photoacoustic Wave Forms. Figure 6 compares the photoacoustic wave form obtained from the reference compound $Co(sen)^{3+}$ to its Fourier transform spectrum. The frequency of the main peak is $3.52 \times 10^6\ s^{-1}$ and corresponds to $\omega_a = 22.1 \times 10^6\ s^{-1}$ or $\nu_a = 3.52$ MHz in eq 1. The shoulders of the Fourier transform spectrum in Figure 6b may be due to the nonideal characteristics of the transducer itself or to the nonideal interfacing between solution and cell wall and/or cell wall and transducer. The results indicate that this particular transducer is best modeled by eq 1 when $\nu_a = 3.52$ MHz and $\tau_0 \cong 1.5$ μs.

The Fourier transforms of several Cr(III) complexes, whose ^2E excited state lifetimes vary from 0.27 to 14 μs, are compared to the $Co(sen)^{3+}$ reference in Figure 7. The band shapes are clearly very similar, and there are no significant frequency changes. Furthermore, the original photoacoustic amplitude and the intensity of its Fourier transform stand in a constant ratio (±3%) independent of the metastable ^2E excited-state lifetimes (Table III).

(21) (a) Langford, C. H.; Vuik, C. P. J. *J. Am. Chem. Soc.* **1976**, *98*, 5409. (b) Langford, C. H.; Malkhasiah, A. Y. S. *J. Chem. Soc., Chem. Commun.* **1982**, 1210.

Table III. Comparison of Experimental Photoacoustic Signal Amplitudes (V_{pa}), Fourier Transform Spectrum Peak Intensity (I), and Metastable Excited-State Lifetimes (τ_2) for Cobalt(III) and Chromium(III) Am(m)ine Complexes

complex	V_{pa}	I	I/V_{pa} (% dev)[a]	τ_2
$Co(sen)^{3+}$	0.425	7.42	17.46 (+2.7%)	$\ll$1 ns
$Cr(NH_3)_5CN^{2+}$	0.207	3.39	16.38 (−3.6%)	14 μs
$Cr(NH_3)_6^{3+}$	0.175	2.91	16.63 (−2.2%)	2 μs
$Cr(NH_3)_5NCS^{2+}$	0.627	11.0	17.54 (+3.2%)	270 ns
av.			17.00	

[a] % dev = $100[(I_a/V_{pa})_{obsd} - (I_a/V_{pa})_{av}]$.

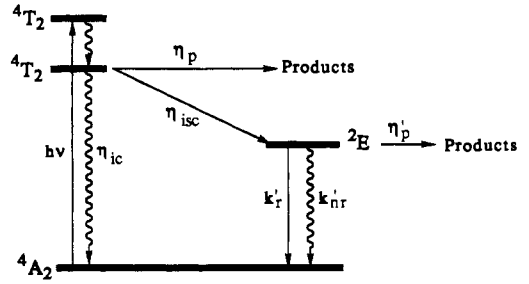

Figure 8. Qualitative energy level scheme for the metal-centered states of a typical Cr(III) complex. We have used the state degeneracies of an octahedral complex for simplicity. Upper (quartet) excited-state processes considered are product formation (η_p), internal conversion (η_{ic}), and intersystem crossing (η_{isc}). The pertinent (^{2}E)Cr(III) excited-state properties are the excited state energy ($E(^2E)$), lifetime ($\tau_2^{-1} = K'_r + K'_{nr} + k'_p$) and product quantum yield (η'_p).

B. Ambient Solution Intersystem Crossing Efficiencies of Some Photoinert Chromium(III) Ammine Complexes with Long-Lived ^{2}E Excited States. If the upper Cr(III) excited states relax efficiently, to populate the (^{2}E)Cr(III) excited state in competition with either population of the ground state or with chemical decomposition (of the upper state) then the sum of efficiencies of all the upper-state processes must equal unity and $\eta_{isc} = 1 - \eta_{ic} - \eta_p$ (see Figure 8; the radiative component, η_r, is ignored since upper-state radiative relaxations are very rare in Cr(III) complexes[11]). If $\eta_p = 0$, then the efficiency of heat released in prompt nonradiative processes of the upper excited states is given by

$$\eta_{pnr} = 1 - \eta_{isc}(E(^2E)/E_{h\nu}) \quad (3)$$

where $E(^2E)$ is the energy of the long-lived ^{2}E excited state and $E_{h\nu}$ is the energy per einstein of photons of frequency ν. The values of η_{pnr} and η_{isc} for several photoinert Cr(III) complexes with long-lived ^{2}E excited states are presented in Table II.

The photoacoustic responses to 462.2-nm excitations of $Cr(bpy)_3^{3+}$ and $Cr(phen)_3^{3+}$ were not well-behaved in that the photoacoustic signal amplitude was not a linear function of the excitation pulse energy (E_p). Rather, we found a significant second-order component as illustrated in Figure 9a. We attribute this behavior to the intense excited-state absorption of the (^{2}E)-Cr(III) polypyridyl complexes in the visible region[22] and thus to the sequential absorption of excitation energy by the ground state and the resulting excited state; e.g.

$$(^4A_2)Cr(bpy)_3^{3+} + h\nu \longrightarrow (^4T_2{}^*)Cr(bpy)_3^{3+} \xrightarrow{\eta_{isc}} (^2E)Cr(bpy)_3^{3+} + \text{heat} \quad (4)$$

$$(^2E)Cr(bpy)_3^{3+} + h\nu \longrightarrow (^2X^*)Cr(bpy)_3^{3+} \quad (5)$$

$$(^2X^*)Cr(bpy)_3^{3+} \longrightarrow \begin{cases} (^2E)Cr(bpy)_3^{3+} + \text{heat} \\ (^4A_2)Cr(bpy)_3^{3+} + \text{heat} \end{cases} \quad (6)$$

where $^2X^*$ is some higher energy excited state (possibly ligand-centered or metal-to-ligand charge transfer) and the secondary

(22) Jamieson, M. A.; Serpone, N.; Hoffman, M. Z. *Coord. Chem. Rev.* **1981**, *39*, 121.

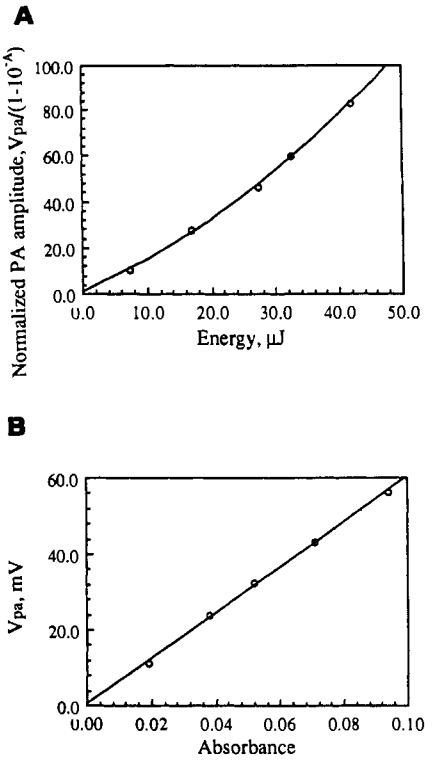

Figure 9. Excitation energy (a) and substrate absorbance (b) dependencies of the photoacoustic signal amplitudes that result from the 462.2-nm irradiations of $Cr(bpy)_3^{3+}$. The solid line in part a, $V_{pa} = 0.925 + 1.206E_p + 0.0178E_p^2$, is fitted to the experimental data (open circles) with a correlation coefficient of 0.999. The solid line in part b, $V_{pa} = 0.5761 + 597.9$ (Abs), is fitted to the experimental data with a correlation coefficient of 0.998.

absorption process (eq 5) returns an additional amount of heat to the solution (eq 6). On the other hand, variations in substrate absorbance with the excitation intensity held constant gave photoacoustic signal amplitudes that were directly proportional to the amount of radiation absorbed (Figure 9b). The signals resulting from a reaction scheme such as described in eqs 4–6, can be represented as

$$V_1 = K_1\eta_1E_p(1 - 10^{-A_1}) \cong K'\eta_1E_pA_1$$

$$V_2 = K_1\eta_2E_p(1 - 10^{-A_2}) \cong K'\eta_2E_pA_2$$

where A_1 and A_2 are the effective absorbances of the ground and excited states, respectively. Since the concentration of excited state was directly proportional to the amount of light absorbed by the substrate, the excited-state absorbance can be represented as $A_2 \cong CA_1E_p$, where C is a constant. In sufficiently dilute solution (total absorbance < 0.1) the observed photoacoustic signal amplitude can be represented as a linear sum of ground-state and excited-state contributions

$$V_{pa} = V_1 + V_2 = K'\eta_1A_1E_p + K'\eta_2CA_1E_p^2 \quad (7)$$

Thus the sequential absorption of two photons by polypyridyl/chromium(III) substrates is consistent with both the nonlinear dependence on excitation pulse energy and the linear dependence on substrate absorbance illustrated in Figure 9. On the basis of the first term in eq 7, we can obtain the nonradiative relaxation efficiency, $\eta_1 = \eta_{pnr}$, and thus the intersystem crossing efficiency, η_{isc}, from eq 3. On the basis of $Cr([9]aneN_3CH_2-)_2^{3+}$ as the reference compound, we find $\eta_{pnr} = 0.35 \pm 0.01$ (average and standard deviation of nine separate determinations) and $\eta_{isc} = 1.03 \pm 0.05$ for $Cr(bpy)_3^{3+}$. This is in excellent agreement with previous reports that $\eta_{isc} = 0.95$–1.00 for this complex (see ref 7a and work cited therein).

C. Bond Dissociation Energies (BDE) of $Cr^{III}(NH_3)_5X$ Complexes in Aqueous Solutions. We have investigated several photoactive chromium(III) complexes with a view of determining the

Table IV. Bond Dissociation Energy Differences for Chromium(III) Ammine Complexes

complex	$\eta(NH_3)^a$	η_{isc}	$\tau(^2E)$,[a] μs	η_{pnr}	ΔH_r, kJ/mol^{-1}	ΔBDE,[b] kJ/mol^{-1}
$Cr(NH_3)_6^{3+}$	0.47[c]	0.75[d]	2.2	0.478 ± 0.010	−11	33 ± 7
$Cr(NH_3)_5Cl^{2+}$	0.37		(2×10^{-6})[e]	1.028 ± 0.015	−20	24 ± 10
$Cr(NH_3)_5CN^{2+}$	0.33		14	0.46		*f*
$Cr(NH_3)_5NCS^{2+}$	0.47		0.27	0.86		*g*

[a] Reference 9 and sources cited therein. [b] ΔBDE = BDE(Cr–NH_3) − BDE(Cr–OH_2). [c] Two photosubstitution pathways have been identified: one that is quenched when (^{2}E)Cr(III) is quenched (η'_p = 0.33) and one that is not quenched (η_p = 0.14). See ref 8 and references cited therein. [d] References 10 and 23 and references cited therein. [e] Value extrapolated from low temperature (<210 K) behavior.[11b] [f] η_{isc} is unknown, but is necessary to calculate ΔBDE. [g] Since τ <300 ns, deconvolution of the photoacoustic transducer wave form is necessary to obtain ΔBDE.

heat changes associated with photosubstitution. The photochemical behavior of these systems can be described in terms of the sequence of steps (when NH_3 photoaquation is much more important than X^- photoaquation)

$$(^4A_2)Cr^{III}(NH_3)_5X + h\nu \rightarrow (^4T_2{}^*)Cr^{III}(NH_3)_5X$$

$$(^4T_2{}^*)Cr^{III}(NH_3)_5X \xrightarrow{\eta_{isc}} (^2E)Cr^{III}(NH_3)_5X$$

$$H_2O + (^4T_2{}^*)Cr^{III}(NH_3)_5X \xrightarrow{\eta_p} (^4A_2)Cr^{III}(NH_3)_4(OH_2)X + NH_3$$

$$(^4T_2{}^*)Cr^{III}(NH_3)_5X \xrightarrow{\eta_{ic}} (^4A_2)Cr^{III}(NH_3)_5X$$

$$H_2O + (^2E)Cr^{III}(NH_3)_5X \xrightarrow{\eta'_p} (^4A_2)Cr^{III}(NH_3)_4(OH_2)X + NH_3$$

$$(^2E)Cr^{III}(NH_3)_5X \xrightarrow{\eta'_{isc}} (^4A_2)Cr^{III}(NH_3)_5X$$

where $\eta_{isc} + \eta_p + \eta_{ic} = 1 = \eta'_p + \eta'_{isc}$, and our observations, summarized in the preceding section, indicate that η_{ic} is usually very small for Cr(III) complexes. All the other steps could in principle contribute to the observed heat pulse following electronic excitation of the substrate. If the product quantum yields, $\eta_p(^4T_2)$ and $\eta'_p(^2E)$, are known for the upper ($^4T_2{}^*$) and lower (^{2}E) energy excited-state substitutional processes and if it is assumed that $\eta_{ic} \cong 0$, then it is possible to determine the heat changes that accompany the photoinduced substitution

$$Cr^{III}(NH_3)_5X + H_3O^+ \xrightarrow{h\nu} Cr^{III}(NH_3)_4(OH_2)X + NH_4^+ + \Delta H_r \quad (8)$$

We have picked several complexes in which the dominant photosubtitution process is ammine hydrolysis (eq 8). There are two metastable excited-state lifetime regimes in which the heat measurements with our system are readily interpretable: (1) $\tau > 3 \times 10^{-7}$ s, and (2) $\tau < 10^{-9}$ s. In the first time regime, the heat produced by the relaxation processes of the ^{2}E excited states do not contribute to the observed photoacoustic signal amplitude, while in the second the observed photoacoustic signal contains both the "prompt" and "slow" heat contributions. The $Cr(NH_3)_6^{3+}$ and $Cr(NH_3)_5CN^{2+}$ complexes fall in the first regime, while $Cr(NH_3)_5Cl^{2+}$ falls in the second and $Cr(NH_3)_5NCS^{2+}$ is intermediate. The efficiencies of heat production from excitation of these complexes (Table IV), η_{pnr}, are ordered as one would expect based on this classification.

For ΔH_r, the heat of the ammine hydrolysis reaction (eq 8), and for a short-lived (^{2}E)Cr(III) excited state (τ < 1 ns), then

$$E_{h\nu} = \eta_{pnr}E_{h\nu} + (\eta_p + \eta'_p)\Delta H_r \quad (9)$$

where $E_{h\nu}$ is the energy per einstein of photons of frequency ν, η_{pnr} is the prompt nonradiative heat emission efficiency, η_{isc} is the intersystem crossing efficiency, η_p is the efficiency of the prompt substitution process and $E(^2E)$ is the energy of the (^{2}E)Cr(III) excited state (note that the upper-state efficiencies are stoichiometrically equivalent to quantum yields). For a long-lived (^{2}E)Cr(III) excited state (τ > 300 ns)

$$E_{h\nu} = \eta_{pnr}E_{h\nu} + \eta_p(\Delta H_r) + \eta_{isc}E(^2E) \quad (10)$$

For $Cr(NH_3)_5Cl^{2+}$ we find ΔH_r = 20 ± 10 kJ mol^{-1}, based on eq 9 and the standard deviation of η_{pnr} as noted in Table IV.

For $Cr(NH_3)_6^{3+}$, there are literature estimates of $\eta_p = 0.14$[9] and $\eta_{isc} = 0.75$.[10,23] Since these values of η_p and η_{isc} do not sum to 1.0, one is led to infer that either (a) there is a significant probability of upper-excited-state relaxation directly to the ground state ($\eta_{ic} \cong 0.11$) for this complex, (b) η_p should be 0.25, or (c) the estimate of η_{isc} should be 0.86. The respective values of ΔH_r based on these three possibilities are as follows: (a) $\Delta H_r{}^a \cong -11 \pm 7$ kJ mol^{-1}; (b) $\Delta H_r{}^b \cong -6 \pm 4$ kJ mol^{-1}; (c) $\Delta H_r{}^c \cong -150 \pm 80$ kJ mol^{-1} (where we have used $E(^2E) = 15.23 \times 10^3$ cm^{-1} in eq 10[10-12]). The first two estimates of ΔH_r are indistinguishable within the estimated assessment of error limits. However, the third possibility considered leads to a physically unreasonable value of ΔH_r = −154 kJ mol^{-1} since this would imply a 111 kJ mol^{-1} stronger Cr–OH_2 bond than the Cr–NH_3 bond. Therefore, we have not listed this as a possible value in Table IV. Further comments pertinent to this issue can be found in the Discussion.

Discussion

We have developed satisfactory approaches to photoacoustic microcalorimetry using visible excitation energies and aqueous solutions by employing several coordination complexes as reference compounds. We have fully characterized our technique through fourier transform analysis of the transducer wave forms and through the experimental determination of the transducer's response to transient heat sources of different lifetimes. The coordination complexes chosen as references are known to be relatively photoinert ($\Phi < 10^{-3}$) and to have subnanosecond intermediate excited-state lifetimes, so that all the initial excitation energy was returned to the solution as heat. The present study has utilized this approach to further characterize the photophysical and photochemical behavior of several chromium(III) am(m)ine complexes.

Transducer Response Characteristics and Their Simulations. The pressure wave (P_{tot}) that is generated when a light pulse passes through a sample solution can, in principle, have contributions from several sources.[2] The most important of these in the systems that we have considered are (a) heat deposition through nonradiative relaxation of molecular excited states (P_{th}), (b) electrostrictive contributions arising from coupling between the electric field vector of light with the solvent dielectric (P_{el}), and (c) the volume changes originating from any photoinduced chemical reactions (P_{ch}). Thus[2]

$$P_{tot} = P_{th} + P_{el} + P_{ch} + \ldots$$

In dilute solutions, P_{el} should be substrate independent, and as illustrated in Figure 9b, this contribution amounts to less than 2 mV (the intercept in figure 9b) in our systems. Only the photoinduced hydrolysis reactions, among those examined here involve a change of volume (note that the molecular geometries of the ^{2}E excited state and the $^4A_2$ ground state of most Cr(III) complexes are nearly identical[9-12,24]). These reactions involve

(23) Endicott, J. F.; Ryu, C. K. *Comments Inorg. Chem.* **1987**, *6*, 91.
(24) Goodman and Herman have reported evidence that the $(^2E)Cr(bpy)_3^{3+}$ excited state is 2 mL mol^{-1} smaller than the $(^4A_2)Cr(bpy)_3^{3+}$ ground state, based on the temperature dependence of photoacoustic signal amplitudes.[6b] Such a value for ΔV_r would result in an underestimate of η_{pnr} by approximately 5%. This is comparable to the experimental uncertainties in our measurement. However, the value of $E(^2E)$ inferred by Goodman and Herman is in error by 30%, and consequently the significance of their value of ΔV_r is not clear.

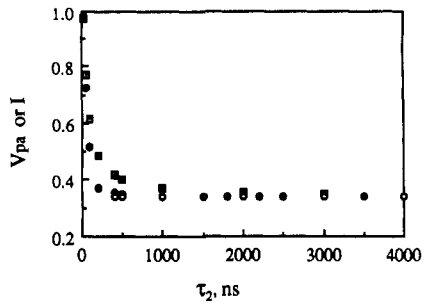

Figure 10. Variations of photoacoustic signal amplitude (V_{PA}) or Fourier transform peak intensity (I) with intermediate lifetimes (a) PA signal amplitude calculated from eq 1 (open squares); (b) experimental PA signal amplitude (open circles); (c) calculated Fourier transform peak intensity based on eq 1 (closed circles). Calculated values from Table I from a "prompt" (τ_u = 10 ps) and a "slow" (τ_2) heat source were used. Experimental data were taken from figure 5.

the substitution of H_2O for a coordinated NH_3. The reactant and product complexes are nearly identical in size and the apparent molal volumes of NH_4^+ and H_3O^+ differ by only about 0.2 mL mol^{-1},[25] so that $\Delta V_r \cong -0.2$ mL mol^{-1}. For irradiations of $Cr(NH_3)_5Cl^{2+}$, the volume change of the photosubstitution reaction is

$$\Delta V_{ch} \cong \alpha l(E_p/E_{h\nu})\Phi_r\Delta V_r$$

where $E_{h\nu}$ is the energy of an eistein of photons, $\Phi_r = 0.14$[9,10] is the photosubstitution quantum yield in water, α is the absorption coefficient, and l is the cell path length. Thus, we estimate $\Delta V_{ch} \cong -1 \times 10^{-12}$ mL for 462.2-nm irradiations of $Cr(NH_3)_5Cl^{2+}$ in water. The volume change for the thermal expansion resulting from heat deposition is $\Delta V_{th} = 2\pi R(\Delta R)l$, where R is the cross-sectional radius and l is the length of the cylinder of solution irradiated by the excitation pulse. Furthermore,[2]

$$\Delta R \cong (E_p\eta_{pnr}\alpha\beta)/(2\pi R\rho C_p)$$

where E_p is the energy of the laser pulse, β is the thermal expansion coefficient of the solvent, ρ is the solvent density, and C_p is the solvent specific heat. Substituting the values of these parameters[26,27] leads to $\Delta V_{th} \cong 6.2 \times 10^{-10}$ mL for our experiments. This corresponding to $P_{ch}/P_{th} \cong 0.2\%$, or about a 2 kJ mol^{-1} underestimate of ΔBDE in the discussion below.

Calculations of the heat response based on eq 1 for a system with one prompt and one slow heat source, typical of Cr(III) complexes, indicate that the second heat source should contribute to the photoacoustic signal amplitude over a very wide range of the metastable excited-state lifetimes, while the intensity of the Fourier transform of the photoacoustic signal should be much less sensitive to contributions from the second heat source. These calculations, summarized in Table I and Figure 10, show that I/I_s values are very close to the input value of 0.340 for the prompt heat source for all values of $\tau_2 \geq 400$ ns, but the calculated value of V_{pa}/V_s shows a 2% deviation even for $\tau_2 = 5$ μs. The experimental signal amplitudes from our transducer are much less sensitive to contributions of the second heat source than is predicted by eq 1, and we find only a 2% deviation of the photoacoustic signal amplitude over whole range of intermediate excited-state lifetimes $\tau_2 \geq 300$ ns (Figures 5b and 10). This insensitivity to the low-frequency heat source may be an intrinsic feature of the narrow band-pass transducer that we have used. We plan to clarify this point in future studies. In any event, it is clear that while eq 1 is a very useful basis for discussing the results of photoacoustic measurements, it should not be expected to always serve as the basis for reliable, detailed analyses of the photoacoustic signal amplitudes or band shapes: (a) comparison of Figures 3 and 6 shows that experimental and theoretical band shapes can differ appreciably; (b) Table I and Figure 10 show that the photoacoustic peak amplitude can be significantly less sensitive to intermediate lifetime than predicted. The experimental characterization of transducer performance is reasonably straightforward, and we have described procedures that can be used for this purpose.

Excited Quartet to Doublet State Intersystem Crossing Efficiencies in Chromium(III) Am(m)ine Complexes. Intersystem crossing from the quartet ligand field excited states ($^4T_2$, $^4T_1$, etc.) to the lowest energy doublet (^2E) appears to be very efficient in chromium(III) complexes.[7,9-11] So far only a complex containing monochlorinated phenanthroline ligands has been shown to exhibit a significant upper-state relaxation pathway that bypasses the doublet manifold ($\eta_{ic} \sim 0.3$).[7a] The only other chromium complex which we have examined that seems to have an intersystem crossing yield that is consistently less than 1.0 is $Cr([9]aneN_3)_2^{3+}$, and even for this complex $\eta_{ic} \leq 0.1$ for the conditions that we have selected. There is a possibility that $Cr(NH_3)_5^{3+}$ has a similar value of η_{ic}, but knowledge of the efficiencies of upper-state chemistry and intersystem crossing is not sufficiently certain for this complex that the internal conversion pathway can be evaluated. Such efficient excited-state quartet-to-doublet spin-relaxation processes are consistent with the picosecond and subpicosecond rise times found for the doublet states of several chromium(III) complexes[28,29] and suggest appreciable electronic coupling between these excited states.[30,31]

Chromium(III)–Ligand Heterolytic Bond Dissociation Energy Differences. The components of the heat change that accompanies photoinduced hydrolysis of an ammine ligand, ΔH_r in eq 8, can be represented in terms of the reactions

$$Cr^{III}(NH_3)_5X(aq) \rightarrow Cr^{III}(NH_3)_5X(g) + \Delta H_1$$

$$Cr^{III}(NH_3)_4(OH_2)X(aq) \rightarrow Cr^{III}(NH_3)_4(OH_2)X(g) + \Delta H_2$$

$$H_2O(aq) \rightarrow H_2O(g) + \Delta H_3$$

$$Cr^{III}(NH_3)_5X(g) \rightarrow Cr^{III}(NH_3)_4X(g) + NH_3(g) + BDE(Cr\text{–}NH_3)$$

$$Cr^{III}(NH_3)_4(OH_2)X(g) \rightarrow Cr^{III}(NH_3)_4X(g) + H_2O(g) + BDE(Cr\text{–}OH_2)$$

$$NH_3(g) \rightarrow NH_3(aq) + \Delta H_4$$

$$H^+(aq) + NH_3(aq) \rightarrow NH_4^+(aq) + \Delta H_5$$

so that $\Delta H_r = \Delta H_1 - \Delta H_2 + \Delta H_3 + \Delta H_4 + \Delta H_5 + BDE(Cr\text{–}NH_3) - BDE(Cr\text{–}OH_2)$. Since the charges and sizes of the two complex cations are about the same, we can assume that $\Delta H_1 \cong \Delta H_2$, and $\Delta H_r \cong \Delta BDE + \Delta H_3 + \Delta H_4 + \Delta H_5$. The three heat quantities are well-known[27] and substituting their values leads to $\Delta BDE = \Delta H_r + 43.5$ kJ mol^{-1}. By this means, we find ΔBDE ≅ 33 kJ mol^{-1} for $Cr(NH_3)_6^{3+}$ and ΔBDE ≅ 24 kJ mol^{-1} for $Cr(NH_3)_5Cl^{2+}$. Correction for the effects of the slightly smaller

(25) Harned, H. S.; Owen, B. B. *The Physical Chemistry of Electrolyte Solutions*; Reinhold: New York, 1958; p 361.
(26) Values of parameters used in these calculations were as follows: E_p = 100 μJ = 10^{-4}J; α = 0.1 cm^{-1}; l = 1 cm; $\beta = 2.57 \times 10^{-4}$ K^{-1};[27] ρ = 0.997 g/mL;[27] C_p = 4.184 J g^{-1} K^{-1};[27] η_{pnr} = 1.028.
(27) Weast, R. C., Astle, M. J., Eds. *CRC Handbook of Chemistry and Physics*, 60th ed.; Chemical Rubber Publ. Co.: Cleveland, OH, 1979–1980.
(28) (a) Kirk, A. D.; Hoggard, P. E.; Porter, G. B.; Rockley, M. G.; Windsor, M. W. *Chem. Phys. Lett.* **1976**, *37*, 199. (b) LeSage, R.; Sala, K., L.; Yip, R. W.; Langford, C. H. *Can. J. Chem.* **1983**, *61*, 2761.
(29) (a) Linck, N. J.; Berens, S. J.; Magde, D.; Linck, R. G. *J. Phys. Chem.* **1983**, *87*, 1733. (b) Rojas, G. E.; Dupuy, C.; Sexton, D. A.; Magde, D. *J. Phys. Chem.* **1986**, *90*, 87.
(30) Typical Stokes shifts (λ_{ss}) of Cr(III) complexes run (3–5) × 10^3 cm^{-1}.[7,10] A simple classical surface-crossing argument would suggest that if there were no electronic prohibition to the intersystem crossing, $k_{isc} \sim \nu_{nu} \exp(-[\lambda_{ss} + E_{Q\text{-}D}]^2/4\lambda_{ss}k_BT) \sim 7 \times 10^{12}$ s^{-1} for a complex with an excited-state quartet–doublet energy difference of 5 × 10^3 cm^{-1} and a coupled nuclear frequency $\nu_{nu} \sim 10^1$ s^{-1}. Strong spin–orbit coupling of the electronic wave functions for these states is expected.[31]
(31) (a) Tanabe, Y. *Prog. Theor. Phys. Suppl.* **1960**, *14*, 17. (b) Sugano, S.; Tanabe, Y.; Kaminura, H. *Multiplets of Transition Metal Ions in Crystals*; Academic Press: New York, 1970.

molar volumes of the products than the reactants would increase these values by approximately 2 kJ mol^{-1}. A simple angular overlap calculation[32-34] leads to 67 and 59 kJ mol^{-1}, respectively. This is surprisingly good agreement with experimental observation for such a crude calculation,[32,35] but more importantly, the AOM calculation supports the inference of a very slightly stronger $Cr-NH_3$ bond in $Cr(NH_3)_6^{3+}$ than in $Cr(NH_3)_5Cl^{2+}$. Our experimental values are also very close to the mean value of ΔBDE ≅ 39.7 kJ mol^{-1} reported for $Co(NH_3)_6^{3+}$ based on conventional thermodynamic measurements.[36]

(32) The small difference in calculated bond energies arises from the contribution of off diagonal elements (σ only) in the secular determinant. Matrix elements were calculated by using tables from Douglas and Hollingsworth[33] and using AOM parameters tabulated by Vanquickenborne and Ceulemans.[34] Note that the $Cr-NH_3$ bond is stronger than the $Cr-OH_2$ bond both in the theoretical calculation and in the experimental measurement.

(33) Douglas, B. E.; Hollingsworth, C. A. *Symmetry in Bonding and Spectra*; Academic Press: New York, 1985; p 243.

(34) Vanquickenborne, L. G.; Ceulemans, A. *Coord. Chem. Rev.* **1983**, *100*, 157.

(35) Note that the assumption that $\Delta H_1 \cong \Delta H_2$ is probably not accurate to the level of a few 10's of kJ mol^{-} found for the differences between the calculated and experimental values of ΔBDE. Similarly, the neglect of electron correlation effects must lead to significant errors in this application of the angular overlap model. It must also be observed that $\Phi(\Delta H_f)$ is determined as the difference between two very large numbers. For example, for $Cr(NH_3)_5Cl^{2+}$, $\Phi(\Delta H_f) \cong -(0.028 \pm 0.01) \times 21.636 \times 10^3$ cm^{-1}. Even if the uncertainty in Φ is negligible, the net uncertainty in ΔH_f is at least 30%.

(36) Christensen, J. J.; Izatt, R. M. Handbook of *Metal Ligand Heats*; Marcel Decker: New York; 1970, p 30.

Contribution from the Department of Chemistry, University of Minnesota, Minneapolis, Minnesota 55455

Common Emissive Intermediates in the Thermal and Photochemical Reactions of Nonemissive Cyclopentadienylruthenium(II) Complexes of Coumarin Laser Dyes

Robert S. Koefod and Kent R. Mann*

Received August 14, 1990

Fluorescent intermediates are observed in the reaction of $[CpRu(CH_3CN)_3]^+$ (Cp = η^5-C_5H_5) with five highly emissive 7-aminocoumarin laser dyes (laser dye = coumarin-334 (10-acetyl-2,3,6,7-tetrahydro-1*H*,5*H*,11*H*-[1]benzopyrano[6,7,8-*ij*]-quinolizin-11-one), coumarin-338 (2,3,6,7-tetrahydro-11-oxo-1*H*,5*H*,11*H*-[1]benzopyrano[6,7,8-*ij*]quinolizine-10-carboxylic acid 1,1-dimethylethyl ester), coumarin-314 (2,3,6,7-tetrahydro-11-oxo-1*H*,5*H*,11*H*-[1]benzopyrano[6,7,8-*ij*]quinolizine-10-carboxylic acid ethyl ester), coumarin-337 (2,3,6,7-tetrahydro-11-oxo-1*H*,5*H*,11*H*-[1]benzopyrano[6,7,8-*ij*]quinolizine-10-nitrile), and coumarin-6 (3-(2-benzothiazolyl)-7-(diethylamino)coumarin). The intermediates exhibit intense, dye-centered absorption and emission bands that are red-shifted 27-79 nm with respect to the free laser dye bands. Similar intermediates are observed when the corresponding nonemissive $[CpRu(\eta^6\text{-laser dye})]^+$ complexes of coumarin-314, coumarin-338, and coumarin-334 are photolyzed in dichloromethane. IR spectral studies suggest that the intermediates contain the laser dye bound to the ruthenium through ligating substituent groups present in the dyes. Both the thermally and photochemically generated intermediates are metastable. The photochemically generated intermediate decays to give free laser dye, while the thermally generated intermediate decays to the $[CpRu(\eta^6\text{-dye})]^+$ complex. This behavior is proposed to result from the relative ability of the differing ancillary ligands present in the thermal and photochemical reactions to stabilize energetic $CpRu^+$ reaction intermediates.

Introduction

Recently, we have been studying compounds of the form $CpRu(arene)^+$ (Cp = η^5-C_5H_5; arene = η^6-arene) that contain the $CpRu^+$ group bound to fluorescent arene ligands such as the 7-aminocoumarin laser dyes. The perturbation of luminescence properties by intermolecular interaction is a well-known phenomenon. Previous studies in our group have demonstrated that the intense emission of these laser dyes is sensitive to changes in the binding of the $CpRu^+$ moiety to the chromophore.[1] This sensitivity to binding is a useful spectroscopic probe for the study of $CpRu^+$-π-ligand chemistry. A major goal of our research is to exploit this spectroscopic sensitivity to detect intermediate species such as a η^4-arene intermediate proposed to occur in the photochemical release of bound arene from $[CpRu(arene)]^+$ in acetonitrile.[2] Toward this goal, we wish to report the observation and spectroscopic characterization of reaction intermediates that occur during both the thermal complexation reaction and the photochemical decomplexation reaction of $CpRu^+$ complexes of certain 7-aminocoumarin laser dyes.

Experimental Section

Dichloromethane was distilled over P_2O_5. Acetone and acetonitrile were of spectroscopic grade and were used without further purification. Laser dyes were obtained from the Eastman Kodak Co. Room-temperature UV-vis spectra of the compounds were obtained with a Cary 17D spectrometer. Rapid-scan UV-vis absorption spectra were collected with a Tracor Northern TN-6500 diode-array apparatus. Emission and excitation profiles were recorded with a Spex F112x spectrofluorometer. ^1H NMR spectra were obtained with an IBM Bruker 200-MHz spectrometer. IR spectra (Mattson Sirius 100 mid-IR spectrometer (120 scans)) of dilute solutions (dichloromethane, 2×10^{-4} M) were obtained of the CpRu-laser dye intermediates with a demountable cell modified with a 0.5-cm Teflon spacer to allow a sufficient path length.

Synthesis of Compounds. $[CpRu(CH_3CN)_3]PF_6$ and the laser dye complexes $[CpRu(coumarin\text{-}1)]PF_6$, $[CpRu(coumarin\text{-}2)]PF_6$, $[CpRu(coumarin\text{-}311)]PF_6$, $[CpRu(coumarin\text{-}344)]PF_6$, $[CpRu(coumarin\text{-}6)]PF_6$, and $[CpRu(coumarin\text{-}388)]PF_6$ were prepared as previously described.[1]

[CpRu(coumarin-334)]AsF_6. The AsF_6^- salt was prepared in the same manner as the PF_6^- salt with the exception that $[CpRu(CH_3CN)_3]AsF_6$ was used in place of $[CpRu(CH_3CN)_3]PF_6$. The NMR, IR, and UV-vis spectra of the cation are identical with those of the PF_6^- compound, and this AsF_6^- salt was used without further characterization.

[CpRu(coumarin-314)]AsF_6. A 20-mL volume of N_2-degassed 1,2-dichloroethane was added to a degassed flask containing 99.9 mg (0.209 mmol) of $[CpRu(CH_3CN)_3]AsF_6$ and 68.0 mg (0.217 mmol) of coumarin-314 (2,3,6,7-tetrahydro-11-oxo-1*H*,5*H*,11*H*-[1]benzopyrano-[6,7,8-*ij*]quinolizine-10-carboxylic acid ethyl ester). The resulting red orange solution was stirred for 3 h. The solvent was removed by rotary evaporation. The residue was dissolved in dichloromethane, and the solution was eluted on a short diatomaceous earth column. Elution with dichloromethane removed the product and left a dark brown impurity on the column. Evaporation of the eluant followed by recrystallization from acetone-ether and washing with ether to remove excess free laser dye yielded 135 mg (0.202 mmol) of dark yellow [CpRu(coumarin-314)]-

* To whom correspondence should be addressed.

(1) Koefod, R. S.; Mann, K. R. *Inorg. Chem.* **1989**, *28*, 2285.

(2) Schrenk, J. L.; McNair, A. M.; McCormick, F. B.; Mann, K. R. *Inorg. Chem.* **1986**, *25*, 3501.

0020-1669/91/1330-2221$02.50/0